THE JOURNAL OF BIOLOGICAL CHEMISTRY VOL. 283, NO. 33, pp. 22847–22857, August 15, 2008
© 2008 by The American Society for Biochemistry and Molecular Biology, Inc. Printed in the U.S.A.

Structural Basis for Sorting Mechanism of p62 in Selective Autophagy*

Received for publication, March 19, 2008, and in revised form, May 19, 2008 Published, JBC Papers in Press, June 4, 2008, DOI 10.1074/jbc.M802182200

Yoshinobu Ichimura[‡1], Taichi Kumanomidou[§1], Yu-shin Sou[‡¶1], Tsunehiro Mizushima[§], Junji Ezaki[‡], Takashi Ueno[‡], Eiki Kominami[‡], Takashi Yamane[§], Keiji Tanaka[¶], and Masaaki Komatsu[‡¶‖2]

From the [‡]Department of Biochemistry, Juntendo University School of Medicine, Bunkyo-ku, Tokyo 113-8421, the [§]Department of Biotechnology, Graduate School of Engineering, Nagoya University, Chikusa-ku, Nagoya 464-8603, the [¶]Laboratory of Frontier Science, Tokyo Metropolitan Institute of Medical Science, Bunkyo-ku, Tokyo 113-8613, and [‖]PRESTO, Japan Science and Technology Corporation, Kawaguchi 332-0012, Japan

Impairment of autophagic degradation of the ubiquitin- and LC3-binding protein "p62" leads to the formation of cytoplasmic inclusion bodies. However, little is known about the sorting mechanism of p62 to autophagic degradation. Here we identified a motif of murine p62 consisting of 11 amino acids (Ser^{334}–Ser^{344}) containing conserved acidic and hydrophobic residues across species, as an LC3 recognition sequence (LRS). The crystal structure of the LC3-LRS complex at 1.56 Å resolution revealed interaction of Trp^{340} and Leu^{343} of p62 with different hydrophobic pockets on the ubiquitin fold of LC3. *In vivo* analyses demonstrated that p62 mutants lacking LC3 binding ability accumulated without entrapping into autophagosomes in the cytoplasm and subsequently formed ubiquitin-positive inclusion bodies as in autophagy-deficient cells. These results demonstrate that the intracellular level of p62 is tightly regulated by autophagy through the direct interaction of LC3 with p62 and reveal that selective turnover of p62 via autophagy controls inclusion body formation.

Macroautophagy (hereafter referred to as autophagy) is a major pathway for intracellular bulk degradation by the lysosome/vacuole, and its molecular machinery is highly conserved among eukaryotes. In the autophagic process, a small membrane sac (called isolation membrane) elongates to enwrap cytoplasmic materials, including organelles, and subsequently the extended membrane closes to form a double-membrane structure termed autophagosome. The autophagosome fuses with the lysosome/vacuole where the sequestered cytoplasmic contents within the autophagosome are degraded by hydrolases of the lysosome/vacuole (1, 2). This system is required to execute turnover of cytosolic proteins and for removal of unwanted organelles (*e.g.* called as pexophagy, mitophagy, and reticulophagy).

Genetic and molecular studies in the yeast *Saccharomyces cerevisiae* have identified 18 *ATG* (autophagy-related genes) essential for autophagosome formation (1). Among them, eight *ATG* products include two ubiquitin-like conjugation systems essential for autophagy (3, 4). Atg12 is a ubiquitin-like protein covalently linked to Atg5 by catalytic reactions of Atg7 (ubiquitin-activating enzyme) and Atg10 (ubiquitin-conjugating enzyme) (5). Atg12-Atg5 interacts with Atg16, resulting in oligomerization of Atg12-Atg5·Atg16 (6). Another ubiquitin-like protein, Atg8 conjugates to a phosphatidylethanolamine (PE).[3] Atg8, synthesized as a precursor form with extra amino acid residues, is processed by Atg4 cysteine protease, which exposes a glycine residue at its C terminus (7). The processed Atg8 is conjugated to PE by Atg7 (ubiquitin-activating enzyme) and Atg3 (ubiquitin-conjugating enzyme) (8). Furthermore, recent studies have revealed that Atg12-Atg5 conjugate functions as a ubiquitin ligase-like enzyme for Atg8 lipidation reaction (9). Finally, the C-terminal glycine of Atg8 covalently conjugates to an amino group of PE (8). Atg8-PE mediates membrane tethering and hemifusion involving the formation of autophagosomal membrane, and its level correlates with autophagosome formation (10). The mammalian Atg8 homologs, microtubule-associated protein 1 light chain 3 (LC3), $GABA_A$ receptor-associated protein (GABARAP), and Golgi-associated ATPase enhancer of 16 kDa (GATE-16), are also conjugated to PE via the same ubiquitin-like system to Atg8 lipidation (11–13).

In recent years, it has become clear that autophagy plays an important role in a variety of physiological responses as follows: starvation, development, differentiation, tumorigenesis, immunity, and neurodegeneration (1). Autophagy, particularly that responsive to starvation, is generally considered a nonselective degradation (1). This large scale degradation enables cells to survive during starvation by recycling of the degradation products for sources of energy production and macromolecule synthesis. In addition to the starvation-induced adaptive autoph-

* This work was supported by grants from the Japan Science and Technology Agency (to M. K.), the Ministry of Education, Science and Culture of Japan (to M. K. and K. T.), the Target Protein Project of Ministry of Education, Science and Culture of Japan (to T. M. and K. T.), and Takeda Science Foundation (to K. T.). The costs of publication of this article were defrayed in part by the payment of page charges. This article must therefore be hereby marked "*advertisement*" in accordance with 18 U.S.C. Section 1734 solely to indicate this fact.

The atomic coordinates and structure factors (code 2ZJD) have been deposited in the Protein Data Bank, Research Collaboratory for Structural Bioinformatics, Rutgers University, New Brunswick, NJ (http://www.rcsb.org/).

[1] These authors contributed equally to this work.

[2] To whom correspondence should be addressed. Tel.: 81-3-3823-2105; Fax: 81-3-3823-2237; E-mail: mkomatsu@rinshoken.or.jp.

[3] The abbreviations used are: PE, phosphatidylethanolamine; LRS, LC3 recognition sequence; LC3, microtubule-associated protein 1 light chain 3; GABARAP, γ-aminobutyric acid, type A, receptor-associated protein; GATE-16, Golgi-associated ATPase enhancer of 16 kDa; MBP, maltose-binding protein; GST, glutathione *S*-transferase; CBB, Coomassie Brilliant Blue; MEF, mouse embryonic fibroblast; GFP, green fluorescent protein; Dox, doxycycline; PB1, Phox and Bem1p.

This is an Open Access article under the CC BY license.

agy, growing lines of evidence point to the importance of basal autophagy that operates constitutively at low rates even under a nutrient-rich environment and plays a vital role in the maintenance of cellular homeostasis (14–17). Indeed, studies using mouse genetics have indicated that autophagy-deficient mice exhibit remarkable accumulation of ubiquitinated protein aggregates followed by hepatocytic and neuronal cell death irrespective of nutrient stresses (14, 15, 17).

p62 is a scaffold protein involved in multiple signaling pathways and is present in ubiquitin-related inclusions such as those seen in liver injury and various neurodegenerative diseases (*e.g.* alcoholic hepatitis, steatohepatitis, Huntington disease, Parkinson disease, and amyotrophic lateral sclerosis) (18–20). Importantly, we have found recently that p62 is a preferred target for autophagy, and intracellular levels of p62 are constantly controlled by constitutive autophagy (21, 22). In addition, previous studies revealed that p62 directly interacts with LC3, an autophagosome marker protein (21, 23). However, little is known molecularly about how p62 is sorted into autophagosomes. In addition to this issue, although we showed that homeostatic levels of p62 control ubiquitin-positive inclusion body formation at the cytoplasm in hepatocytes and neurons of autophagy-deficient mice (21), it is still unclear whether inclusion formation is only because of deficiency in p62 turnover. In other words, the molecular relationship between autophagic removal of p62 and inclusion body formation remains to be uncovered.

This study was designed to shed light on the aforementioned issues related to p62, LC3, autophagosome, inclusion formation, and autophagy. We report the identification of LC3 recognition sequence (LRS) of p62, which includes 11 amino acids (Ser^{334}–Ser^{344}), and the crystal structure of LC3-LRS complex, clarifying the interaction mode at the molecular level. Further biochemical and genetic analyses using autophagy- and/or p62-deficient mouse cells demonstrated that autophagic degradation of p62 absolutely depends on the interaction of LC3, and that the impairment of the physical interaction leads to the formation of cytosolic inclusion bodies. The results indicate that p62 is essential for inclusion body formation associated with impaired autophagy.

EXPERIMENTAL PROCEDURES

Plasmid Construction—Maltose-binding protein (MBP) fused p62 (MBP-p62), and its deletion mutant (MBP-p62M7) expression plasmids have been described previously (21). To construct p62M7 variants, a series of deletions of p62M7 were amplified by PCR using appropriate primers and cloned into the MBP fusion expression plasmid, pMALp2 (New England Biolabs). Glutathione *S*-transferase (GST)-fused LC3B expression plasmid has been described previously (13). Point mutations were inserted by the QuikChange site-directed mutagenesis kit (Stratagene) according to the protocol supplied by the manufacturer. All constructs were confirmed by DNA sequencing with BigDye terminator cycle sequencing ready reaction kit version 1.1 (Applied Biosystems).

Purification of Recombinant Proteins for Pulldown Experiments—MBP-tagged p62 and mutants were expressed in *Escherichia coli* strain BL21 Star (DE3) (Invitrogen) by induction of 0.05 mM isopropyl β-D-thiogalactopyranoside at 25 °C for 16 h. The cells were lysed in bacterial protein extraction reagent (Pierce) at room temperature for 10 min. Insoluble proteins were removed by centrifugation at 15,000 rpm for 10 min by microcentrifuge. The cell extracts were diluted 1:5 into TBS (20 mM Tris-HCl, pH 7.5, and 150 mM NaCl) and incubated with amylose resin (New England Biolabs) at 4 °C for 2 h. The MBP fusion protein-bound amylose resins were washed three times with TBS. The MBP-p62 and mutants were eluted with TBS containing 10 mM maltose. The purity was confirmed on SDS-polyacrylamide gel followed by Coomassie Brilliant Blue (CBB) staining (SimplyBlue SafeStain (Invitrogen)). GST-tagged LC3, its mutants GABARAP and GATE-16, were purified in a manner similar to that described above except for affinity purification using glutathione-Sepharose 4B (Amersham Biosciences). For removal of the GST region, PreScission protease cleavage was performed (Amersham Biosciences). Protein concentrations were determined by BCA protein assay reagent (Pierce).

Pulldown Assay—MBP-p62 and its mutants were expressed in *E. coli* BL21 Star (DE3), and the cell extracts were prepared by bacterial protein extraction reagent. The cell extracts were diluted 5-fold with TBS and incubated with amylose resin (New England Biolabs). The MBP-p62 and its mutants immobilized amylose resin were washed extensively with TBS. The resulting immobilized amylose resins containing about 5 μg of MBP fusion proteins were incubated with 15 μg of LC3 family proteins (LC3, GABARAP, or GATE-16) in 50 μl of TBS on ice for 1 h, and then washed three times with 500 μl of TBS. Bound proteins with amylose resins were suspended into SDS-PAGE sample buffer and subjected to SDS-PAGE followed by CBB staining. GST pulldown was performed through the same procedures described above, except that GST fusion was immobilized on glutathione-Sepharose 4B (Amersham Biosciences), and MBP-p62M7 was introduced in this assay.

Protein Expression and Purification for Crystal Structure—GST-tagged LC3 was expressed from pGEX6P plasmid in BL21 (RIPL). The protein was purified using glutathione-Sepharose 4B and cation exchange chromatography. The GST moiety was proteolytically removed by PreScission protease. The protein solution was concentrated to 18.6 mg/ml by ultrafiltration in 25 mM Tris-HCl, pH 7.5, and 1 mM dithiothreitol. The concentrated LC3 was mixed with LRS peptide representing residues ^{334}SGGDDDWTHLS^{344} from p62 with equal molar ratio and incubated for 3 h.

Crystallization and Data Collection—Crystals of LC3-LRS peptide complex were obtained at 15 °C by the hanging-drop vapor-diffusion method, with a mixture of 2.0 μl of protein and the same volume of reservoir solution (0.1 M HEPES, pH 7.5, and 25% w/v polyethylene glycol 3,350). Although crystals formed in 2 days, they were not sufficient for crystal structure determination. Initial crystals were used to generate larger crystals by microseeding. During the microseeding experiments, the concentration of the precipitant was varied. Single crystals suitable for x-ray diffraction measurement were finally obtained with reservoir conditions consisting of 0.1 M HEPES, pH 7.5, and 23% w/v polyethylene glycol 3,350. Crystals were transferred to cryoprotective solution containing 10% v/v glyc-

TABLE 1
Data collection and refinement statistics
Values in parentheses represent highest resolution shell.

	LC3-p62 (334–344)
Data collection	
Space group	$P2_1$
Cell dimensions	
a, *b*, *c* (Å)	45.6, 39.6, 78.0
α, β, γ (°)	90.0, 93.3, 90.0
Wavelength (Å)	0.9000
Resolution (Å)	1.55 (1.61-1.55)
Total reflections	179,556
Unique reflections	39,943
Completeness (%)	98.4 (86.0)
$I/\sigma(I)$	23.9
Multiplicity	4.5 (4.2)
R_{merge}	0.054 (0.310)
Refinement	
Resolution range (Å)	77.85–1.56
R_{work}/R_{free}	0.199/0.237
Root mean square deviation	
Bonds (Å)	0.010
Angles (°)	1.298

erol, 0.1 M HEPES, pH 7.5, and 23% w/v polyethylene glycol 3,350 for 30 s.

Diffraction data sets for the LC3-p62 complex were collected at 100 K on beamline BL44XU (SPring-8, Japan). Data processing and reduction were carried out with the DENZO/SCALEPACK (36). The crystal forms of LC3-p62 complex belong to the $P2_1$ space group and two molecules in the asymmetric unit. Data collection, phasing, and refinement statistics are summarized in Table 1.

Structure Determination and Refinement—The structure of the LC3-p62 complex was determined by molecular replacement using MOLREP (32) with LC3 (PDB ID code 1UGM) (29) as a search model. An initial model was constructed using ARP/wARP (37). Manual building was then carried out using the program XtalView (38) and altered with several cycles of refinement using the program REFMAC5 (39). The final refined model consists of residues 2–122 and residues 1–122 of the molecules in the asymmetric unit. For the p62 peptide, the density allowed building 10 residues complexed to one molecule and 7 residues complexed to the second molecule. Phasing and refinement statistics are summarized in Table 1. There were no residues in the disallowed regions of the Ramachandran plot. Structure figures were generated using CCP4MG (40) and PyMOL (41).

Generation of Tet-On Cells—Immortalized *p62-* and *Atg7/p62*-deficient mouse embryonic fibroblasts (MEFs) were established by infecting MEFs with a recombinant retrovirus carrying a temperature-sensitive simian virus 40 large T antigen (42). Tetracycline-mediated p62-expressing cell lines were generated using the reverse tetracycline-regulated retroviral vector (43). A cassette consisting of the gene-encoding packaging signal (ψ), the reverse tetracycline-controlled transactivator (rtTA), the internal ribosome entry site from the encephalomyocarditis virus, the blasticidin S deaminase, a heptamerized tetracycline operator sequence (tetO), the minimal human cytomegalovirus immediate early promoter designated P_{hcmv}*-1 (CMV), and green fluorescent protein (GFP)-fused mouse p62 cDNA or various p62 mutants (p62W340A, p62L343A, p62D338A/D339A, and p62D337A/D338A/D339A) were cloned into a Moloney murine leukemia virus retroviral vector pLXSN backbone (43). Retrovirus packaging cells, PLAT-E (44), transfected with the vectors were cultured at 37 °C for 24 h. After changing the medium, the virus producing PLAT-E was further incubated at 37 °C for 24 h. The viral supernatant was collected and used immediately for infection. The immortalized *p62-* and *Atg7/p62*-deficient MEFs were plated on 35-mm dishes in 3 ml of growth medium at 24 h before infection. Just before infection, the medium was replaced with undiluted viral supernatant with 8 μg/ml Polybrene (Sigma). Twenty four hours later, the cells were introduced into the selection medium containing 5 μg/ml of blasticidin S (Invitrogen). The cells remaining after 5 days were used in the experiments. To induce the expression of p62, the cells were treated with 250 μg/ml of doxycycline (Dox, Sigma) for 24 h.

Immunological Analysis—MEFs were lysed with lysis buffer (10 mM Tris-Cl, pH 7.4, 150 mM NaCl, Complete protease inhibitor mixture (Roche Diagnostics), and 2% Triton X-100). The lysates were centrifuged at 15,000 rpm for 5 min at 4 °C, and the resultant supernatant was analyzed by immunoblotting. The antibodies for p62, Atg7, and LC3 were described previously (21). The antibody for actin (MAB1501R) was purchased from Chemicon International. For immunofluorescence microscopy, MEFs grown on glass coverslips were immunostained with anti-LC3 (21) and anti-ubiquitin antibodies (FK2, MBL) as described previously (21).

Accession Codes—Protein Data Bank: The coordinates and structure factors for LC3-LRS complex have been deposited under accession code 2ZJD.

RESULTS

LC3-interacting Region of p62—p62 is composed of three domains as follows; N-terminal Phox and Bem1 (PB1) domain, zinc finger domain (Zinc), and C-terminal ubiquitin-associated (UBA) domain (19, 20). Several reports have suggested that p62 can directly interact with LC3, thereby possibly sequestering p62 into the autophagosome (21, 23). We have shown previously that LC3 interacts with a linker region (named M7 domain) between the zinc finger and UBA domain in mouse p62 (21). To determine the minimal region of p62M7-(168–391) required for the interaction with LC3, we performed pulldown assay experiments using a series of deletion mutants of p62M7. Initially, we examined six mutants of truncated p62M7 (M71–M76) (Fig. 1*A*). Each MBP-fused p62M7 mutant (M71–M76), which was immobilized on amylose resins, was incubated with recombinant LC3B (hereafter referred to as LC3), washed extensively, and subjected to SDS-PAGE followed by CBB staining. LC3 was clearly detected in pulldown products with p62 mutants harboring the M76 region (334–391) but not the M72 region (168–333), suggesting that p62M76-(334–391) is sufficient for the interaction with LC3 (Fig. 1*B*). To shorten the interaction domain, we subsequently prepared a deletion series of p62M76 (M77–M82) for MBP pulldown assay. These pulldown assays revealed that p62M82, which includes 11 amino acids (334–344), is essential and sufficient for LC3 interaction (Fig. 1*B*). p62M82, which we named LRS (LC3 recognition sequence), contains two conserved motifs across species as

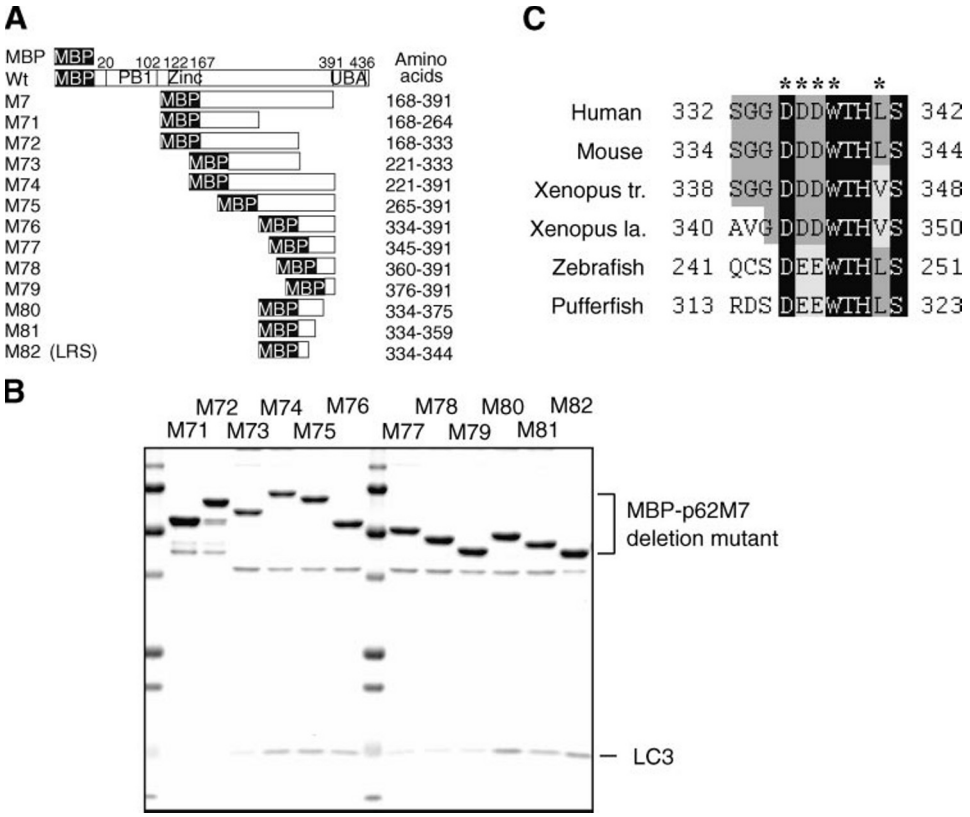

FIGURE 1. **Identification of LC3-interacting region in p62.** *A,* diagrams of deletion-mutation constructs of p62 used for the pulldown assay. The MBP-tagged mouse p62(Wt) and its deletion mutants p62M7 have been described previously (21). Deletions of M7 (M71–M82) were generated by PCR amplifications and fused to the C terminus of MBP. Phox and Bem1p (*PB1*), zinc finger (*Zinc*), and ubiquitin-associated (*UBA*) domains are represented. LRS; LC3 recognition sequence means the LC3 binding region (334–344) in p62. *B,* MBP pulldown assay. MBP-p62M7 deletion mutants conjugated with amylose resins were incubated with purified recombinant LC3. The pulled down complex with MBP-p62M7 mutants was subjected to SDS-PAGE and visualized by CBB staining. *C,* LRS alignment of p62 homologs in various species. *Asterisks* indicate LC3-interacting residues; *black* and *gray boxes* indicate identical amino acid residues with complete and partial conservation, respectively.

follows: acidic cluster (337–339) DDD (or DEE) and hydrophobic residues (340 and 343) W*XX*L (or W*XX*V) involved in protein-protein interaction (Fig. 1*C* and see also Fig. 2).

Overall Structure of the LC3-LRS Complex—Based on the above results, we determined the structure of LC3-LRS complex by x-ray crystallography. The complex consists of a full-length LC3-(1–125) bound to the LRS of p62-(334–344). The crystal structure of the LC3-LRS complex was determined by molecular replacement using C-terminal truncated LC3-I (residues 1–120, PDB code 1UGM) and refined to 1.56 Å resolution (Fig. 2*A*). The final model consists of residues 2–122 and residues 1–122 of the two molecules in the asymmetric unit (molecules A and B), respectively. The structure of LRS-bound LC3, which consists of a five-stranded β-sheet and five α-helices, is essentially identical to the previously reported structures of peptide-free LC3-I; these structures have an average 1.15 Å root mean square deviation for the C-α positions, although several differences are evident. The LRS binds to one side of the LC3 surface opposite the C-terminal region. Of the 11 residues in the LRS crystals, only 10- and 7-residue segments (molecule A, 335–344; molecule B, 338–344) are ordered in the structure. The LC3 surface has a narrow channel, and the LRS binds within the LC3 groove in an extended conformation (Fig. 2*B*). The LRS-binding surface consists of three α-helices (α1, α2, and α3) and two β-strands (β1 and β2). A total of 601 Å^2 of accessible surface area is buried at the interface between the LC3 and LRS. The most striking feature of the interactions is that the indole ring of Trp^{340} is inserted into a site surrounded by a conserved group of hydrophilic and hydrophobic residues, Asp^{19}, Ile^{23}, Pro^{32}, Lys^{51}, Leu^{53}, and Phe^{108} (Fig. 2, *B–D*). The second major interaction is between Leu^{343} of LRS and the β1, β2, and α3 of LC3. Leu^{343} makes van der Waals contacts with Ile^{35}, Phe^{52}, Val^{54}, Leu^{63}, and Ile^{66} and the aliphatic portion of the Arg^{70} (Fig. 2, *B–D*). The third interaction site is between the N-terminal portion of LRS and the basic cluster (Arg^{10}, Arg^{11}, and Lys^{49}) on the surface of LC3. A group of charged and hydrophilic residues are present in the contact area for both interacting partners that could potentially form a series of salt bridges and hydrogen bonds between the two molecules. These hydrophilic contacts include Asp^{337} and Asp^{338} from LRS and Arg^{10} and Arg^{11} of LC3. In addition, the peptide is coordinated by several hydrogen bonds involving Asp^{337}, Thr^{341}, Leu^{343}, and Ser^{344} of LRS and Lys^{51}, Leu^{53}, and Arg^{69} of LC3.

To confirm the interacting structure of LC3-LRS, point mutation was inserted into the indicated amino acids of LRS in p62M7 by replacement with alanine (Fig. 2*E*). MBP pulldown assay showed that the formation of the LC3-p62M7 complex was significantly reduced in W340A and L343A mutants (Fig. 2*E*). Likewise, the interaction with LC3 was almost abolished in D337A/D338A, D338A/D339A, and D337A/D338A/D339A mutants (Fig. 2*E*). These results indicate that the hydrophobic (Trp^{340} and Leu^{343}) and acidic cluster (Asp^{337}–Asp^{339}) of p62 are important for LC3 binding. The structure of LC3-LRS suggests that the LRS associates with many amino acids of LC3. In the next step, we introduced mutation in a number of these amino acids of LC3 critically involved in the interaction with LRS as follows: R10A, R11A, K51A, F52A, L53A, I66A, R70A, and N-terminal helix deletion ($\Delta\alpha$1 or $\Delta\alpha$1-α2), followed by GST pulldown assay (Fig. 2*F*). As predicted from the crystal structure of the complex, the series of GST-LC3 mutants tested were significantly compromised in their ability to pull down MBP-p62M7 (Fig. 2*F*). These results are in agreement with the above results of crystal structure analysis.

Predicted Structures of Atg8 Homolog-LRS Complex—The sequence homology between LC3 and other Atg8 homologs suggests that LRS may also bind to other Atg8 homologs (Fig.

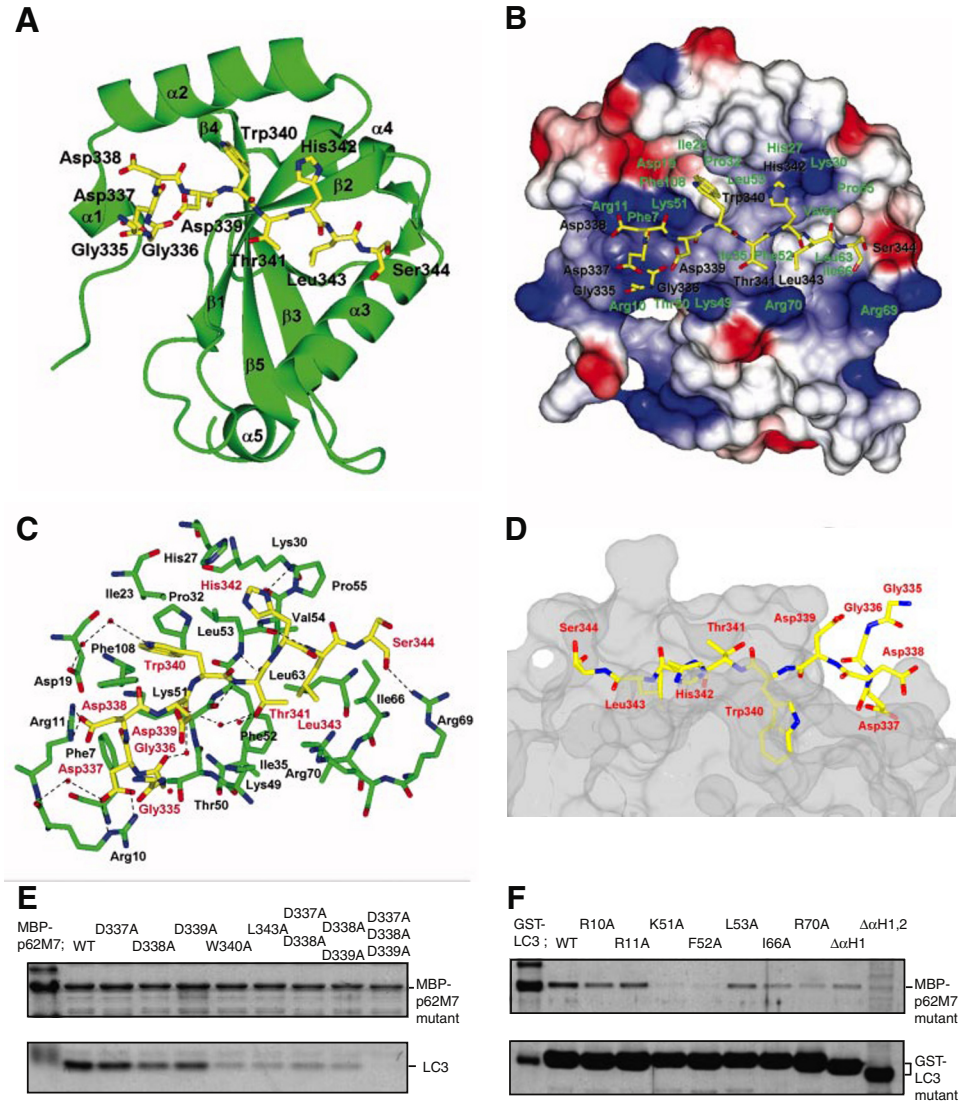

FIGURE 2. **Structure of the LC3-p62 peptide complex.** *A,* overall structure of the complex. *Green,* LC3 color; *yellow,* p62 peptide (LRS). The secondary structure elements (α1–α5 helices and β1–β5 sheets) for LC3 are labeled. *B,* electrostatic surface representation of the p62-binding site of the LC3 with the LRS. The surface is colored according to the electrostatic potential (*blue,* positive; *red,* negative). Residues from LC3 that interact with p62 are labeled in *green*. *C,* close-up view of the LC3-LRS interface showing amino acids of LC3 (*green*), LRS (*yellow*), and water molecules (*red*). *Dashed lines,* hydrogen bonds. *D,* side view with partial transparency of the LC3-LRS interaction. Stick of LRS (*yellow*) is shown within the groove of LC3 molecular surface (partially *transparent gray*). *E,* pulldown assay with p62M7 mutants. MBP-p62M7 mutants immobilized amylose resin, and purified LC3 was incubated, and the pulled down products were subjected to SDS-PAGE followed by CBB staining. *F,* pulldown assay with LC3 mutants. GST-LC3 mutants immobilized glutathione-Sepharose 4B, and purified p62M7 were incubated, and then the pulled down products were subjected to SDS-PAGE followed by CBB staining.

3*A*). To elucidate the binding mode between LRS peptide and Atg8 homologs, the complex models of GABARAP-LRS and GATE-16-LRS were created from the rat GABARAP (24) and bovine GATE-16 (25) structures, respectively, by using the MOE program (version 2005.06; Chemical Computing Group, Montreal, Canada) (Fig. 3, *C* and *D*). In these models, although GABARAP and GATE-16 form the major interaction sites of Trp^{340} and Leu^{343}, the basic surface on α1 helix of LC3 interacting with the acidic cluster of Asp^{337}–Asp^{339} are different from those of the corresponding GABARAP and GATE-16 region (Fig. 2*B* and Fig. 3, *C* and *D*). However, MBP pulldown assay showed the equivalent interactions of p62M7 with LC3, GABARAP, and GATE-16 (Fig. 3*B*) suggesting that Atg8 homologs have a similar affinity for p62 in the *in vitro* condition.

Interaction between LC3 and p62 Is Indispensable for in Vivo Autophagic Degradation of p62—To investigate the degradation mode of p62 by autophagy (*i.e.* via interaction with LC3) *in vivo*, we took advantage of the Tet-On system (Fig. 4*A*). The Tet-On/Tet-Off system allows regulation of reversible and quantitative gene expression in cells. The Tet-On system is widely used to induce gene expression by treatment of cells with tetracycline or its analog Dox (26). We prepared a regulator gene cassette, CAG-rtTA and TRE-GFP-fused wild type and a series of p62 mutants (W340A, L343A, D338A/D339A, and D337A/D338A/D339A), and then introduced them into immortalized *p62* knock-out and *Atg7/p62* double knock-out mouse embryonic fibroblasts (MEFs) to abolish the effect of endogenous wild-type p62. The presence of Dox in the culture medium should induce the expression of GFP-p62 and the mutants, whereas Dox removal should allow suppression of the expression (Fig. 4*A*). To examine the degradation of p62, the cells were cultured in media containing Dox for 24 h, and then the level of GFP-p62 was chased for 36 h by culturing Dox-free media. Both wild-type and mutant GFP-p62 were efficiently expressed in each cells (Fig. 4, *B* and *C*). Removal of Dox markedly decreased the expression of wild-type GFP-p62 in *p62*$^{-/-}$ MEFs by 12 h, and this fall was time-dependent, and only small amounts of GFP-p62 (9.76%) remained at 36 h after removal of Dox. In contrast, such down-regulation was trivial and insignificant in *Atg7/p62* double knock-out MEFs (Fig. 4, *B* and *C*); 75.9% of GFP-p62 remained even at 36 h after removal of Dox in double knock-out MEFs. These results indicate that the degradation of GFP-p62 is mainly dependent on the autophagy pathway. When the mutant forms of GFP-p62, which has a slight binding capacity to LC3 (Fig. 2*E*), were expressed into *p62*$^{-/-}$ MEFs, the rates of the degradation were much slower compared with that of wild-type p62 (Fig. 4, *B* and *C*). The percentages of p62W340A, p62L343A, p62D338A/D339A, and p62D337A/D338A/D339A remaining at 36 h after removal of Dox were 44.6, 48.1, 49.0, and 49.6%, respectively. However, these remaining levels were still lower than that of

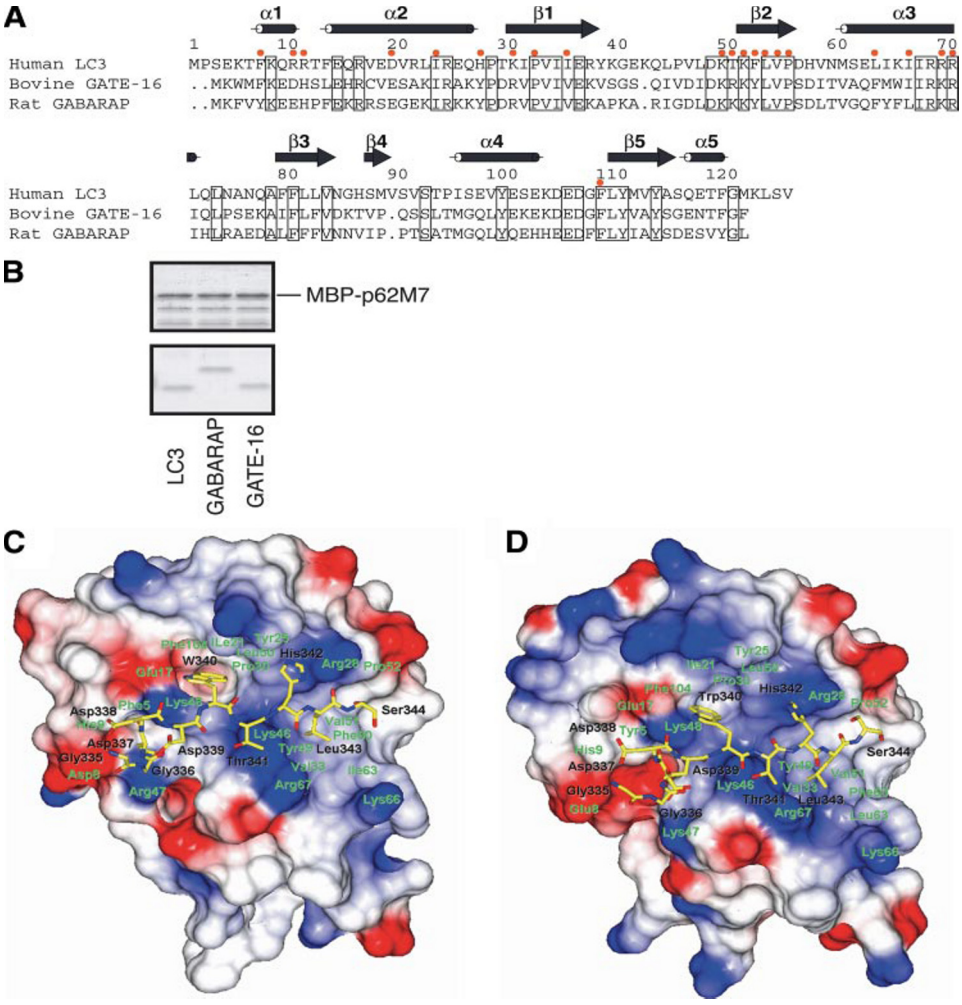

FIGURE 3. **Comparison of LC3 and its homologs.** *A,* sequence alignments of human LC3, rat GABARAP, and bovine GATE-16. Identical amino acid residues are *boxed*. The secondary structural element of LC3 is indicated *above* the alignments. LC3 interacting residues of p62 peptide are indicated by *red circles*. *B,* interaction of p62M7 and LC3 homologs. MBP-p62M7 conjugated with amylose resins were incubated with purified LC3, GABARAP, and GATE-16. The pulled down products with MBP-p62M7 were detected in CBB-stained SDS-PAGE. *C* and *D,* models of the GATE-16-p62 peptide and GABARAP-p62 peptide complex from published structures (codes 1eo6 and 1kgt). GATE-16 and GABARAP are shown in electrostatic surface representation. p62 peptide is shown as a *stick model*. Residues that correspond to residues from LC3 shown in Fig. 2*B* are labeled.

GFP-p62 in *Atg7/p62* double knock-out MEFs, implying partial defect in degradation of these mutants. Interestingly, an *in vitro* binding assay revealed no significant difference in the LC3-binding ability among p62 mutants except for the triple D337A/D338A/D339A mutant accompanied with severely reduced LC3 interaction (Fig. 2*E*). However, these degradation rates *in vivo* were almost similar, suggesting equal contribution among hydrophobic (Trp^{340} and Leu^{343}) and acidic (Asp^{337}–Asp^{339}) clusters of p62 on LC3 interaction *in vivo*. Taken together, these *in vivo* results strongly suggest that loss of interaction between LC3 and p62 is sufficient to impair the degradation of p62.

PB1 Domain of p62 Is Important for Efficient Degradation of p62 via Autophagy—The PB1 domains are scaffold modules that adopt the topology of ubiquitin-like β-grasp folds with the interaction of each other in a front-to-back mode to arrange heterodimers or homo-oligomers (27). Actually, p62 can polymerize via the PB1 domain (28). To examine the roles of the PB1 domain in autophagic degradation of p62, we expressed a K7A/D69A mutant of p62, which compromises the interaction surface of the PB1 domain, accompanied with loss of self-oligomerization activity (28), in $p62^{-/-}$ MEFs using the Tet-On system, and then compared the degradation rate of the mutant with that of wild-type p62. Surprisingly, this mutation was accompanied by significantly degradative delay, compared with wild-type p62 (Fig. 4, *D* and *E*). The percentages of wild-type and p62K7A/D69A remaining at 36 h after removal of Dox was 7.80 and 36.9%, respectively. However, the degradation rate of p62K7A/D69A in $p62^{-/-}$ MEFs was still higher than that in *Atg7/p62* double knock-out MEFs, indicating that the defective oligomerization form of p62 is still degraded, at least in part, by the autophagy pathway (Fig. 4, *D* and *E*). Actually, additional mutation of p62 lacking LC3 interaction accelerated the delay of degradation (Fig. 4, *D* and *E*). These results suggest that in addition to LC3 interaction, self-oligomerization of p62 is required for effective degradation of p62 via autophagy.

Impairment of LC3-p62 Interaction Causes Ubiquitin- and p62-positive Inclusion Formation—Finally, we investigated the cellular localization of wild-type p62 and the mutants. Consistent with previous studies (21, 22), immunofluorescent analysis with anti-LC3 antibody showed localization of GFP-p62 in cup-shaped and dot structures in GFP-p62-expressing *p62* knock-out MEFs. These structures were always positive for LC3 (Fig. 5*A*). Impairment of p62 turnover by autophagy deficiency causes accumulation of p62-positive inclusion (21). Indeed, 20–30% of *Atg7/p62* double knock-out GFP-p62-expressing MEFs contained GFP-p62-positive inclusions characterized by their large sizes and positive staining for anti-ubiquitin (Fig. 5*B*). Similarly, expression of GFP-p62 mutants, which have lower ability to associate with LC3 (Fig. 2*E*), was associated with the formation of p62-positive inclusions, although these inclusions were almost negative for LC3 (Fig. 5*A*). Moreover, ubiquitinated proteins were also present in the structures (Fig. 5*B*). In *p62* knock-out MEFs expressing GFP-p62, only a few ubiquitin-positive dots were detected in autophagosomes positive for GFP-p62, suggesting that the ubiquitin-positive aggregates in MEFs might be trapped into autophagosomes before they become large aggregates/inclusions. Both auto-

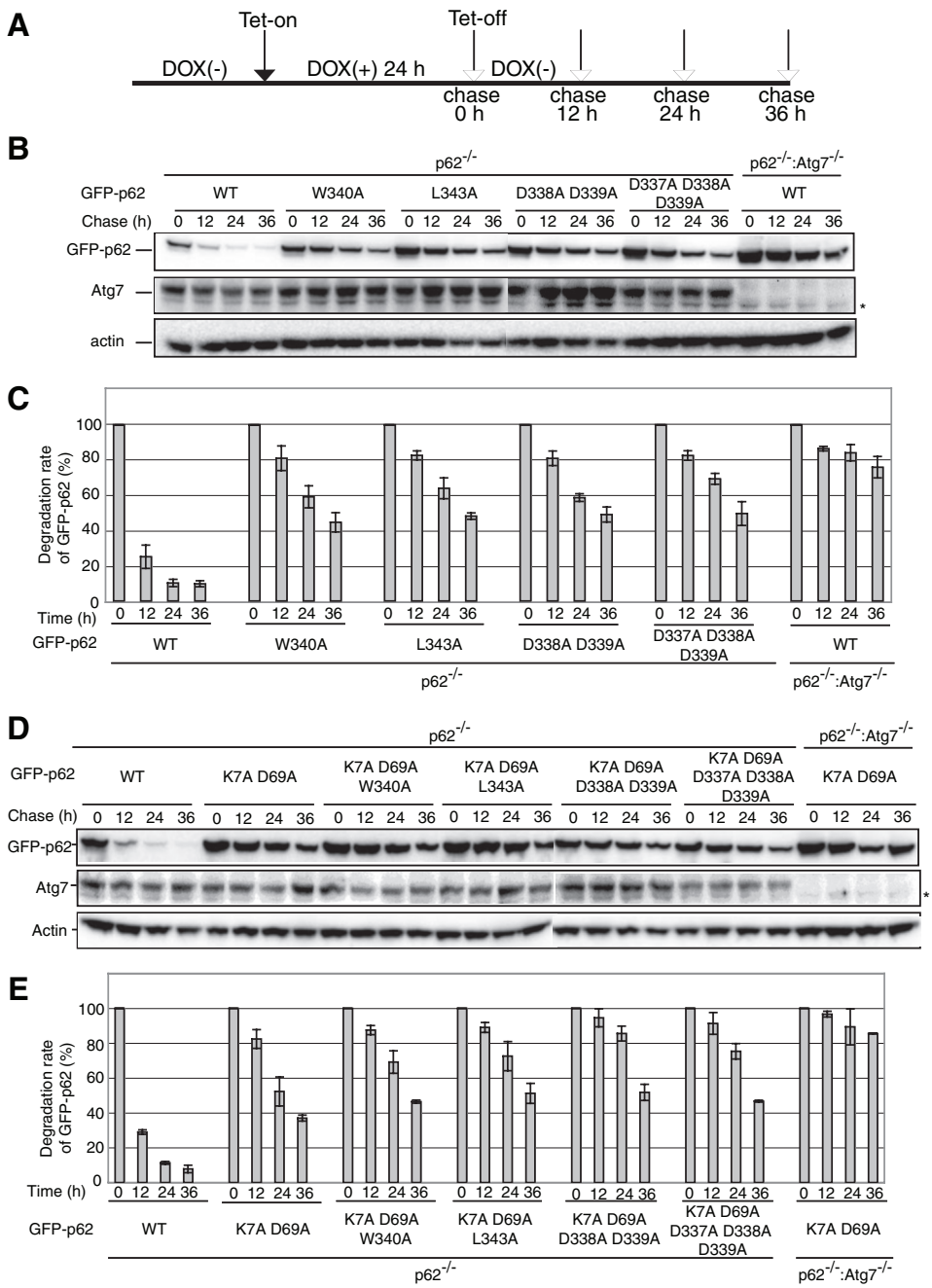

FIGURE 4. **Turnover of p62 is dependent on interaction with LC3 and p62.** *A,* schematic representation of experiments conducted to monitor p62 protein level. Immortalized *p62* and *Atg7/p62* knock-out MEFs were introduced with two regulator gene cassettes, CAG-rtTA and TRE-GFP-fused wild type and a series of mutant p62 (p62W340A, p62L343A, p62D338AD339A and p62D337AD338AD339A) with or without PB1 mutation (K7AD69A). These cells were cultured for 24 h in the presence of Dox to induce expression of GFP-p62 or the mutants. Subsequently, the cells were cultured in the absence of Dox and lysed at the times indicated by *white arrows. B,* immunoblot analysis of GFP-p62. The cell lysates were prepared at various time points after transient expression of GFP-p62 and the mutants and then subjected to SDS-PAGE followed by immunoblotting with the indicated antibodies. Data are representative of three separate experiments. *Asterisk,* nonspecific band. *C,* quantitative densitometry of immunoblotting data shown in *B* and the ratios of p62 relative to actin. *D,* immunoblot analysis of GFP-p62 with PB1 mutation. GFP-p62K7AD69A with or without mutation of LC3 interaction was expressed into immortalized *p62* and *Atg7/p62* knock-out MEFs and analyzed as shown in *A. E,* quantitative densitometry of immunoblotting data shown in *D* and the ratios of p62 relative to actin.

phagosome formation and degradation of long lived proteins in *p62* knock-out cells are apparently comparable with those in wild-type cells (21). These results therefore indicate that impairment of p62-LC3 interaction alone is sufficient for the formation of ubiquitin- and p62-positive inclusions, *i.e.* loss of the interaction triggers inclusion body formation.

Based on the possible oligomerization in PB1 domain and the ubiquitin-binding ability in the UBA domain of p62, it is postulated that PB1 plays an important role in inclusion formation, including polyubiquitinated proteins. Indeed, when GFP-p62K7AD69A lacking self-oligomerization activity was expressed into *Atg7/p62* double knock-out MEFs, inclusion formation observed in those expressing wild-type p62 was completely suppressed (Fig. 5*C*), strongly suggesting the essential role of the PB1 domain in inclusion formation (for details see "Discussion").

DISCUSSION

We have reported recently that the intracellular level of p62 is controlled by constitutive autophagic degradation, and impairment of such a process causes significant accumulation of inclusion bodies containing p62 and ubiquitinated proteins (21). Furthermore, we and Pankiv *et al.* (21, 23) found that p62 interacts directly with LC3, an autophagosome marker protein. These reports imply that p62 could be targeted to the autophagosome through interaction with LC3 for degradation of itself together with ubiquitinated proteins. However, information on the sorting mechanism(s) for p62 is not available at present.

We originally identified the LRS consisting of 11 amino acids in p62. The short peptide of p62, LRS, allowed us to determine the crystal structure of the LC3-LRS complex. The tertiary structure of LC3-LRS revealed that both acidic cluster (DDD or DEE) and hydrophobic motif (W*XX*L or W*XX*V) in LRS are highly conserved among species and involved in the interaction with LC3. Recently, Pankiv *et al.* (23) reported the LC3 interacting region (LIR) consisting of 22 amino acids (Arg^{321}–Ser^{342}) in human p62. In comparison, the LRS (Ser^{334}–Ser^{344}) in murine p62 described in the present study is shorter than the LIR but corresponds exactly to the

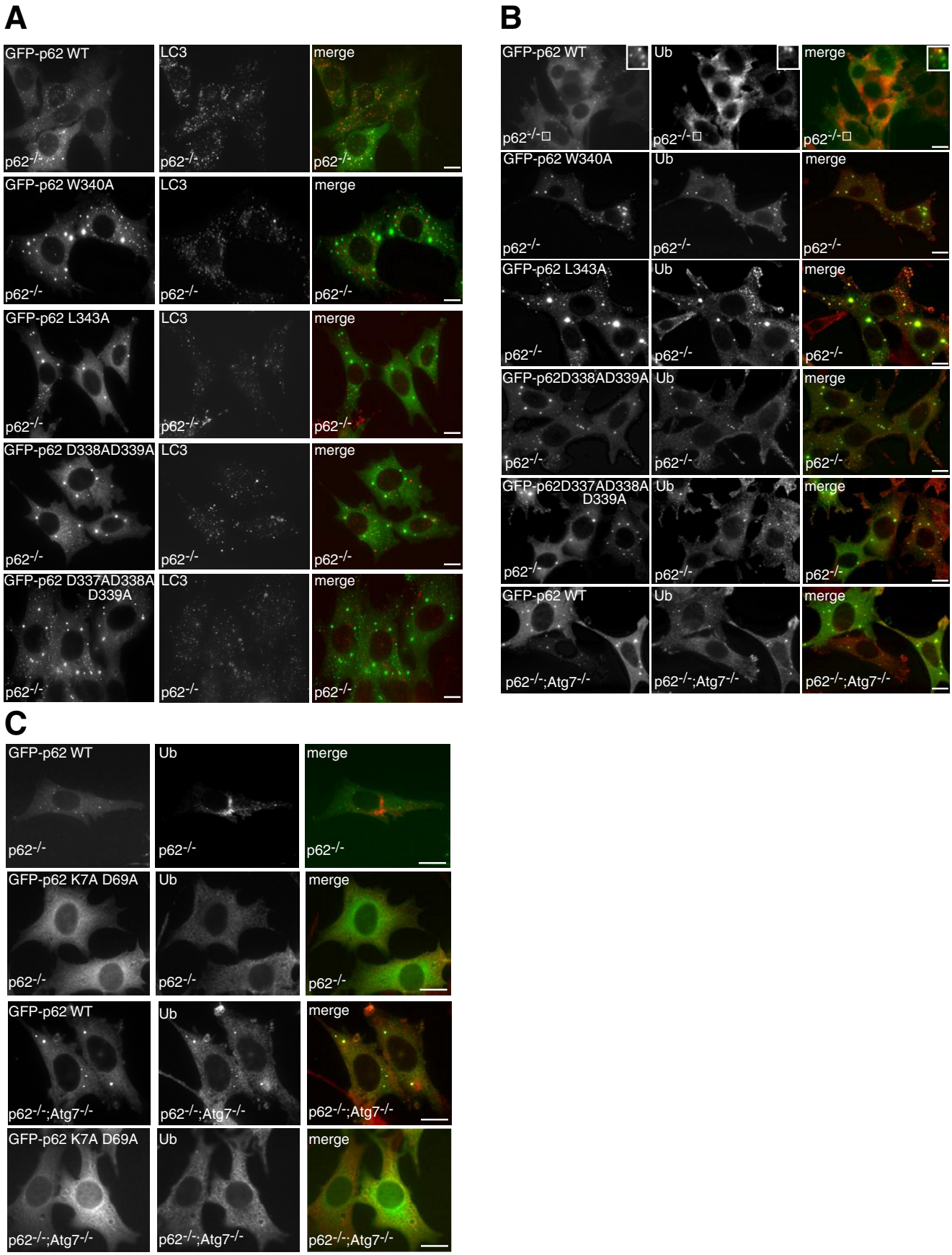
A
GFP-p62 WT
LC3
merge
p62-/-
GFP-p62 W340A
GFP-p62 L343A
GFP-p62 D338AD339A
GFP-p62 D337AD338A D339A
B
Ub
p62-/-□
p62-/-;Atg7-/-
C
GFP-p62 K7A D69A

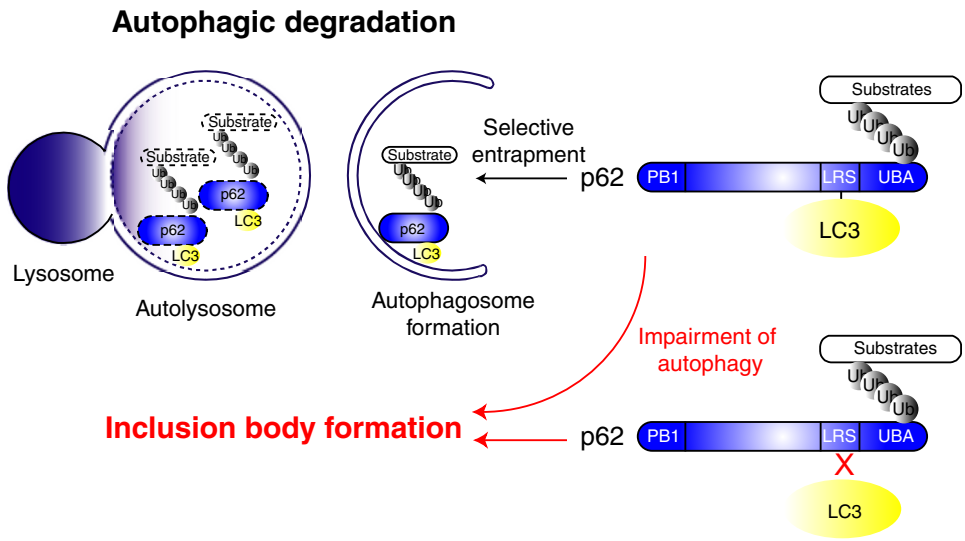

FIGURE 6. **Schematic model for selective autophagy mediated by p62.** p62 was dissected into three domains in the context of the present study, *i.e.* N-terminal PB1 for self-oligomerization, LRS for LC3 interaction, and C-terminal UBA for ubiquitin binding domains. Ubiquitinated proteins initially interact with the UBA domain and are selectively entrapped into autophagosomes through interaction between LRS and LC3 for their degradation under normal conditions. Because PB1 mutant (K7A/D69A) lacking self-oligomerization ability was associated with decreased degradation of itself, oligomerization of p62 might be needed for effective turnover of p62. On the other hand, impaired turnover of p62 (*e.g.* genetic loss of autophagy or mutation of LRS in p62 in our hand) causes accumulation of p62 associated with ubiquitinated proteins, resulting in high cytoplasmic levels of p62, which presumably promote self-oligomerization of p62 via the PB1 domain. Subsequently, those oligomer complexes segregate and form inclusion bodies in the cytoplasm to reduce the cytotoxic effects of soluble and/or oligomerized proteins. Note that the LRS mutant of p62 lacking LC3 binding ability induces significant inclusion body formation, analogous to that in autophagy-deficient cells. Accordingly, the interaction between LC3 and p62 is a key event in selective autophagy that contributes to the aggressive removal of unfavorable ubiquitinated proteins in cells.

C-terminal region of LIR (23). In addition, their mapping of the sites involved in LC3 interaction is also essentially similar to our results except the importance of Leu^{343} residue found in our study (23).

The structure of LC3 includes a C-terminal ubiquitin fold and N-terminal two α-helices (29). In this study, we identified a new functional molecular surface composed of N-terminal basic residues and two hydrophobic pockets at the ubiquitin domain of LC3 as p62-interacting regions. The two distinct hydrophobic pockets were present close to each other on the surface of the ubiquitin fold and just localized at the interface of the complex. Previous mutational analyses of Atg8 identified the critical residues involved in autophagosomal membrane formation (10, 30). Intriguingly, Lys^{48}–Leu^{50} of Atg8, essential for autophagosome formation after PE conjugation reaction, corresponds to Lys^{51}–Leu^{53} existing in the two hydrophobic pockets of LC3 (10, 30). Similarly, the N-terminal two α-helices of LC3, corresponding to the region involved in tethering and hemifusion function of Atg8, are also required for p62 interaction (10). These results suggest that both autophagosome formation and p62 recognition utilize a common hydrophobic patch on the LC3 surface.

The structure of GABARAP has been shown in two conformations as follows: one is the N-terminal α-helix connected to the ubiquitin domain (closed), and the other is the N-terminal α-helix projected away from ubiquitin domain (open) (31). Furthermore, we have proposed that PE conjugation induces conformation change in the N-terminal α-helices of Atg8, and the open form is active conformation for hemifusion (10). These findings suggest that the region of the N-terminal α-helices of Atg8 is flexible. Because the structure of the LC3-LRS complex exists in a form in which basic residues of the N-terminal of LC3 bind to the acidic cluster of LRS, the LC3 N-terminal α-helices might be stabilized as a closed (or inactive) form. Conceivably, the two distinct conformations with the N terminus of LC3 may be related to the underlying molecular functions such as membrane expansion and/or sorting receptor in autophagy.

Structure comparison of LRS-bound LC3 homologs has shown high similarity and LRS structurally aligned on the two hydrophobic pockets on their ubiquitin fold surface (24, 25, 29). Interestingly, the basic amino acids in the N-terminal helices of LC3 are not found in those of other Atg8 homologs, suggesting that LC3 might have a higher affinity for p62 than other homologs. However, we have not detected any differences among LC3 homologs in the *in vitro* pulldown experiments, implying the similar affinity of LC3 homologs for p62. Although GABARAP and GATE-16 share common biochemical characteristics with LC3 and localize to autophagosomes (3, 12), their behaviors responding to nutrient conditions differ among Atg8 homologs (17). Further analysis is required to unravel the structural relationship of interaction between Atg8 homologs and p62.

We have shown that autophagy deficiency leads to marked accumulation of p62- and ubiquitin-positive inclusion, and p62 is indispensable for such inclusion formation (21). Importantly, p62 is a major component of ubiquitin-containing inclusions known as the "hepatocytic Mallory body" found in alcoholic hepatitis and steatohepatitis (32). Similar structures have been identified also as proteinaceous aggregates in the remnant neu-

FIGURE 5. **Impairment of p62-LC3 interaction is sufficient to induce the formation of ubiquitin- and p62-positive inclusions.** *A,* immunofluorescence analysis of cellular localization of GFP-p62 and LC3. *p62* knock-out MEFs were fixed at 36 h after transient expression of GFP-p62 and the mutants and then immunostained with anti-LC3 antibody. *Right panels,* merged images. *Bar,* 10 μm. *B,* immunofluorescence analysis of cellular localization of GFP-p62 and ubiquitin. *p62* or *p62/Atg7* knock-out MEFs were fixed as shown in *A* and then immunostained with anti-ubiquitin antibody. *Right panels,* merged images. Higher magnification views in *top panels* are shown in *insets*. *Bar,* 10 μm. *C,* immunofluorescence analysis of cellular localization of GFP-p62 and GFP-p62K7A/D69A. *Atg7/p62* knock-out MEFs were fixed at 36 h after transient expression of GFP-p62 or GFP-p62K7A/D69A and then immunostained with anti-ubiquitin antibody. *Right panels,* merged images. *Bar,* 10 μm.

rons in various neurodegenerative disorders such as Parkinson disease and amyotrophic lateral sclerosis (33, 34). In such diseases, it is plausible that the reduced autophagic activity is associated with the formation of inclusion bodies. This possibility is also supported by the results of a recent study using CHMP2B mutants (35). However, it remains unclear whether only impairment of p62 turnover through autophagy is responsible for the formation of inclusion bodies. Our analyses using the Tet-On system clearly showed delayed degradation of p62 mutants lacking LC3 interaction when they were expressed in *p62* knock-out MEFs, resulting in the formation of inclusions containing ubiquitinated proteins. It is noteworthy that autophagosome formation and degradation of long lived proteins in *p62* knock-out cells are comparable with those in wild-type cells (21). Therefore, it seems that only impairment of p62-LC3 interaction is responsible for ubiquitin- and p62-positive inclusion formation.

How is p62 involved in the formation of ubiquitin-positive inclusion? Currently, it is known that the UBA domain of p62 interacts with ubiquitinated proteins (19, 20, 23). However, ubiquitin-tagged proteins are not aggregation-prone themselves. Therefore, it is plausible that excess accumulation of p62 interacting with ubiquitinated protein might predispose to form inclusions via the PB1 domain, which retains the ability of self-oligomerization. Indeed, p62 having PB1 mutation (K7A/D69A), which is defective in self-oligomerization, did not form inclusions in *Atg7* knock-out cells, and then the ubiquitinated proteins remained dispersed, indicating that oligomerization of p62 through the PB1 domain is critical for ubiquitin-positive inclusion in autophagy-deficient cells.

Therefore, it is clear that under physiological conditions, ubiquitinated proteins initially interact with p62 via the UBA domain, and are subsequently selectively entrapped into the autophagosomes through LRS-LC3 interaction for their degradation (see the schematic illustration in Fig. 6, *top panel*). On the other hand, impaired autophagy under certain pathological conditions leads to the accumulation of p62-ubiquitinated protein complexes followed by oligomerization via the PB1 domain, ultimately leading to the formation of inclusion body that presumably contributes to the segregation of harmful and/or unnecessary proteins within the cell (Fig. 6, *bottom panel*). This scenario is in agreement with the previous observations that almost all inclusions in autophagy-deficient cells were positive for both p62 and ubiquitin (21), and reduction of p62 protein level increased cell death when a harmful mutant of Huntingtin was overexpressed (22). Taken together, our results indicate that p62 directly binds to LC3 and is targeted to constitutive and selective autophagy to maintain an intracellular homeostatic level of p62.

Acknowledgments—We thank T. Kouno for the excellent technical assistance; Dr. N. Furuya for helpful discussion; Dr. T. Kitamura (Tokyo University) for providing the PLAT-E cells; Dr. M. Hagiwara (Tokyo Medical and Dental University) for providing the pLRT-X retrovirus vectors; and Dr. Z. Yue (Mount Sinai School of Medicine) for the critical reading of the manuscript.

REFERENCES

1. Levine, B., and Klionsky, D. J. (2004) *Dev. Cell* **6,** 463–477
2. Mizushima, N. (2007) *Genes Dev.* **21,** 2861–2873
3. Ohsumi, Y. (2001) *Nat. Rev. Mol. Cell Biol.* **2,** 211–216
4. Suzuki, K., and Ohsumi, Y. (2007) *FEBS Lett.* **581,** 2156–2161
5. Mizushima, N., Noda, T., Yoshimori, T., Tanaka, Y., Ishii, T., George, M. D., Klionsky, D. J., Ohsumi, M., and Ohsumi, Y. (1998) *Nature* **395,** 395–398
6. Kuma, A., Mizushima, N., Ishihara, N., and Ohsumi, Y. (2002) *J. Biol. Chem.* **277,** 18619–18625
7. Kirisako, T., Ichimura, Y., Okada, H., Kabeya, Y., Mizushima, N., Yoshimori, T., Ohsumi, M., Takao, T., Noda, T., and Ohsumi, Y. (2000) *J. Cell Biol.* **151,** 263–276
8. Ichimura, Y., Kirisako, T., Takao, T., Satomi, Y., Shimonishi, Y., Ishihara, N., Mizushima, N., Tanida, I., Kominami, E., Ohsumi, M., Noda, T., and Ohsumi, Y. (2000) *Nature* **408,** 488–492
9. Hanada, T., Noda, N. N., Satomi, Y., Ichimura, Y., Fujioka, Y., Takao, T., Inagaki, F., and Ohsumi, Y. (2007) *J. Biol. Chem.* **282,** 37298–37302
10. Nakatogawa, H., Ichimura, Y., and Ohsumi, Y. (2007) *Cell* **130,** 165–178
11. Kabeya, Y., Mizushima, N., Ueno, T., Yamamoto, A., Kirisako, T., Noda, T., Kominami, E., Ohsumi, Y., and Yoshimori, T. (2000) *EMBO J.* **19,** 5720–5728
12. Kabeya, Y., Mizushima, N., Yamamoto, A., Oshitani-Okamoto, S., Ohsumi, Y., and Yoshimori, T. (2004) *J. Cell Sci.* **117,** 2805–2812
13. Sou, Y. S., Tanida, I., Komatsu, M., Ueno, T., and Kominami, E. (2006) *J. Biol. Chem.* **281,** 3017–3024
14. Hara, T., Nakamura, K., Matsui, M., Yamamoto, A., Nakahara, Y., Suzuki-Migishima, R., Yokoyama, M., Mishima, K., Saito, I., Okano, H., and Mizushima, N. (2006) *Nature* **441,** 885–889
15. Komatsu, M., Waguri, S., Chiba, T., Murata, S., Iwata, J., Tanida, I., Ueno, T., Koike, M., Uchiyama, Y., Kominami, E., and Tanaka, K. (2006) *Nature* **441,** 880–884
16. Komatsu, M., Ueno, T., Waguri, S., Uchiyama, Y., Kominami, E., and Tanaka, K. (2007) *Cell Death Differ.* **14,** 887–894
17. Komatsu, M., Waguri, S., Ueno, T., Iwata, J., Murata, S., Tanida, I., Ezaki, J., Mizushima, N., Ohsumi, Y., Uchiyama, Y., Kominami, E., Tanaka, K., and Chiba, T. (2005) *J. Cell Biol.* **169,** 425–434
18. Zatloukal, K., Stumptner, C., Fuchsbichler, A., Heid, H., Schnoelzer, M., Kenner, L., Kleinert, R., Prinz, M., Aguzzi, A., and Denk, H. (2002) *Am. J. Pathol.* **160,** 255–263
19. Moscat, J., Diaz-Meco, M. T., and Wooten, M. W. (2007) *Trends Biochem. Sci.* **32,** 95–100
20. Seibenhener, M. L., Geetha, T., and Wooten, M. W. (2007) *FEBS Lett.* **581,** 175–179
21. Komatsu, M., Waguri, S., Koike, M., Sou, Y. S., Ueno, T., Hara, T., Mizushima, N., Iwata, J., Ezaki, J., Murata, S., Hamazaki, J., Nishito, Y., Iemura, S., Natsume, T., Yanagawa, T., Uwayama, J., Warabi, E., Yoshida, H., Ishii, T., Kobayashi, A., Yamamoto, M., Yue, Z., Uchiyama, Y., Kominami, E., and Tanaka, K. (2007) *Cell* **131,** 1149–1163
22. Bjørkøy, G., Lamark, T., Brech, A., Outzen, H., Perander, M., Overvatn, A., Stenmark, H., and Johansen, T. (2005) *J. Cell Biol.* **171,** 603–614
23. Pankiv, S., Clausen, T. H., Lamark, T., Brech, A., Bruun, J. A., Outzen, H., Øvervatn, A., Bjørkøy, G., and Johansen, T. (2007) *J. Biol. Chem.* **282,** 24131–24145
24. Bavro, V. N., Sola, M., Bracher, A., Kneussel, M., Betz, H., and Weissenhorn, W. (2002) *EMBO Rep.* **3,** 183–189
25. Paz, Y., Elazar, Z., and Fass, D. (2000) *J. Biol. Chem.* **275,** 25445–25450
26. Gossen, M., and Bujard, H. (1992) *Proc. Natl. Acad. Sci. U. S. A.* **89,** 5547–5551
27. Moscat, J., Diaz-Meco, M. T., Albert, A., and Campuzano, S. (2006) *Mol. Cell* **23,** 631–640
28. Lamark, T., Perander, M., Outzen, H., Kristiansen, K., Øvervatn, A., Michaelsen, E., Bjørkøy, G., and Johansen, T. (2003) *J. Biol. Chem.* **278,** 34568–34581
29. Sugawara, K., Suzuki, N. N., Fujioka, Y., Mizushima, N., Ohsumi, Y., and Inagaki, F. (2004) *Genes Cells* **9,** 611–618
30. Amar, N., Lustig, G., Ichimura, Y., Ohsumi, Y., and Elazar, Z. (2006)

EMBO Rep. **7,** 635–642
31. Coyle, J. E., Qamar, S., Rajashankar, K. R., and Nikolov, D. B. (2002) *Neuron* **33,** 63–74
32. Stumptner, C., Fuchsbichler, A., Heid, H., Zatloukal, K., and Denk, H. (2002) *Hepatology* **35,**1053–1062
33. Kuusisto, E., Salminen, A., and Alafuzoff, I. (2001) *Neuroreport* **12,** 2085–2090
34. Nakano, T., Nakaso, K., Nakashima, K., and Ohama, E. (2004) *Acta Neuropathol.* **107,** 359–364
35. Filimonenko, M., Stuffers, S., Raiborg, C., Yamamoto, A., Malerød, L., Fisher, E. M., Isaacs, A., Brech, A., Stenmark, H., and Simonsen, A. (2007) *J. Cell Biol.* **179,** 485–500
36. Otwinowski, Z., and Minor, W. (1997) *Methods Enzymol.* **276,** 307–326
37. Vagin, A., and Teplyakov, A. (1997) *J. Appl. Crystallogr.* **30,** 1022–1025
38. Morris, R. J., Perrakis, A., and Lamzin, V. S. (2003) *Methods Enzymol.* **374,** 229–244
39. McRee, D. E. (1999) *J. Struct. Biol.* **125,** 156–165
40. Murshudov, G. N., Vagin, A. A., and Dodson, E. J. (1997) *Acta Crystallogr. Sect. D Biol. Crystallogr.* **53,** 240–255
41. Potterton, E., McNicholas, S., Krissinel, E., Cowtan, K., and Noble, M. (2002) *Acta Crystallogr. Sect. D Biol. Crystallogr.* **58,** 1955–1957
42. Delano, W. L. (2002) *The PyMOL Molecular Graphics System,* DeLano Scientific, San Carlos, CA
43. Lee, G. H., Ogawa, K., and Drinkwater, N. R. (1995) *Am. J. Pathol.* **147,** 1811–1822
44. Watsuji, T., Okamoto, Y., Emi, N., Katsuoka, Y., and Hagiwara, M. (1997) *Biochem. Biophys. Res. Commun.* **234,** 769–773